

Dual Role for Heterogeneity in Dynamic Fracture

Itamar Kolvin*

School of Physics, Georgia Institute of Technology, 837 State St NW, Atlanta, 30332, GA, USA

Mokhtar Adda-Bedia

Laboratoire de Physique, CNRS, ENS de Lyon, Université de Lyon, F-69364 Lyon, France

(Dated: July 3, 2024)

Are heterogeneous materials harder to break than homogeneous ones? Predicting rapid crack propagation in the presence of inhomogeneities remains a challenge. Linear perturbations leave the net speed of fracture unchanged. We obtain a nonlinear equation of motion for planar crack fronts to gain insight into the dynamic fracture of moderately heterogeneous solids. The coupling of the front geometry to the heterogeneity landscape renormalizes the energy dissipation and the crack velocity. In materials whose toughness is weakly sensitive to crack speed, such as silica glass, heterogeneity results in increased dissipation and slower crack propagation. However, heterogeneity has a reduced effect and may even facilitate fracture in strongly velocity-dependent materials.

Keywords: Fracture mechanics, heterogeneous materials, dynamic fracture, nonlinear dynamics

Introduction. Heterogeneous materials that locally vary in their mechanical properties are everywhere in geology [1–6], biology [7], and engineering [8–10]. The bulk properties of heterogeneous media, such as the Young modulus, are known to be well-represented by macroscopic averaging over the material microstructure [11]. In contrast, the consequences of heterogeneity in fracture are only beginning to be ascertained. The challenge in predicting the toughness of heterogeneous media is the need to resolve three-dimensional crack propagation in space and time [12–17].

Heterogeneity may produce toughening effects. Quasi-static cracks experience local and transient arrests at tough asperities, also termed “strong pinning” [18–21]. In bulk fracture, the formation of complex out-of-plane surface structure may be triggered by inhomogeneities [22–25]. The resultant growth in fracture surface area is associated with increased energy dissipation [17, 25, 26]. Still, the impact of heterogeneity on the resistance of materials to *dynamic* cracks remains an open question. Existing computational methods, including the spectral boundary integral method [27], phase field simulations [25, 28–30] and atomistic models [31, 32], predict 3D crack motion by obtaining the full elastic fields. The need to resolve 3D or 2D dynamic fields that are nearly singular close to the crack tip limits the accessible system sizes. Thus, approaching the thermodynamic limit of 3D heterogeneous fracture remains a challenge.

To make progress, we analytically approximated the elastic fields near planar cracks at the 2nd-order in the crack front fluctuation [33]. The local balance between the elastic energy flux and dissipation dictated a one-dimensional equation of motion for the crack front. Solutions for cracks traversing heterogeneous media showed that, beyond mere averaging, crack front fluctuations renormalize the global dissipation and speed of fracture. In materials of weakly velocity-dependent tough-

ness, such as silica glass [34], dynamic cracks are slower and dissipate more energy than predicted by the average toughness. The opposite is true, however, for sufficiently rapid cracks in materials of strongly velocity-dependent toughness, as are silicon [35], plastics [34] and polymer gels [16, 36].

Crack front equation of motion. Dynamic cracks are governed by the balance $G = \Gamma$, between the elastic energy per unit area flowing into the crack tip, G , and the dissipation per unit area tied to the creation of new surfaces, Γ [13, 16, 33]. To investigate how dynamic cracks interact with inhomogeneities, the dependence of G and Γ on the crack front geometry, velocity, and history is needed. Consider a semi-infinite crack lying in the $y = 0$ plane of a linearly elastic solid subject to remote tensile stresses. In the absence of heterogeneity, the crack front is straight and propagates at velocity V along the x axis. Asymptotically ahead of the crack tip, the tensile stress at the fracture plane is singular $\sigma_{yy} \sim (x - Vt)^{-1/2}$. The energy released per unit area is $G = G_r g(V)$, where G_r depends on the loading conditions and $g(V)$ is a universal function that regulates the flow of energy into the crack tip [37]. For a crack front whose position at time t and at coordinate z is $x = Vt + f(z, t)$, energy balance becomes

$$G_r g(V)(1 + \delta G) = \Gamma(x, z; V_\perp), \quad (1)$$

where $\Gamma(x, z; V_\perp)$ captures the toughness heterogeneity and dependence on the local normal crack velocity $V_\perp(z, t) = (V + \partial_t f) / \sqrt{1 + (\partial_z f)^2}$. The energy release rate fluctuation δG is a nonlinear functional of $f(z, t)$ and its derivatives that may be approximated by a perturbation expansion [12–14, 33, 38, 39].

How do small local variations in Γ modify the crack dynamics? The linear response of dynamic crack fronts to perturbations is known [13, 15, 38]. Let us decompose the crack front fluctuation into Fourier components $\hat{f}(k, \omega) = \int dz dt e^{-ikz - i\omega t} f(z, t)$. For small f , Ramanathan and

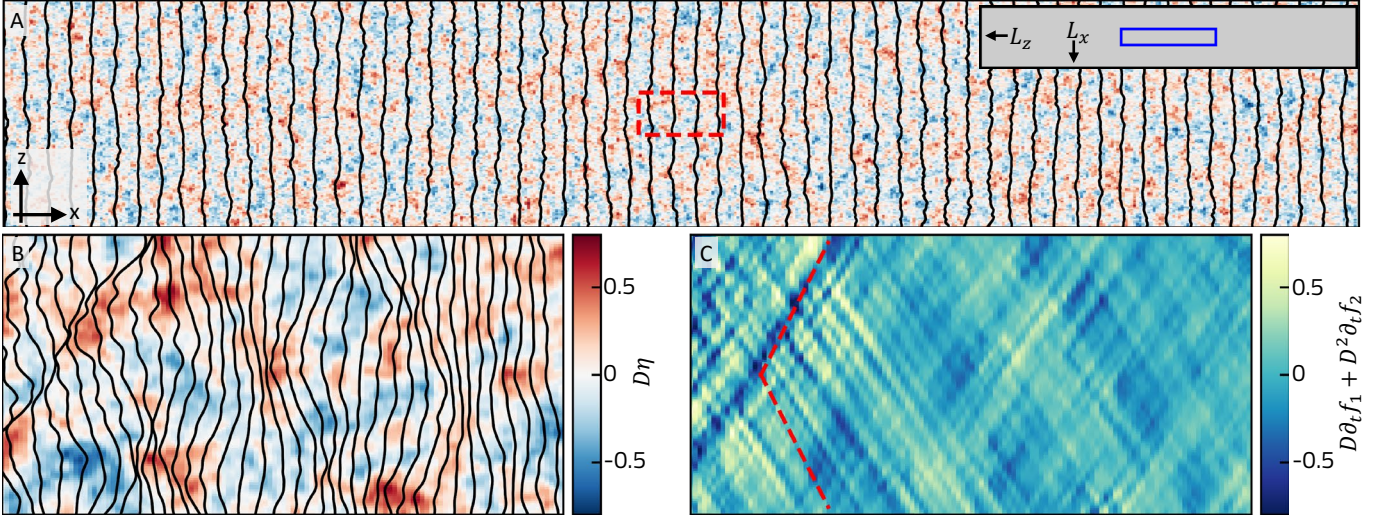


FIG. 1. **Crack front dynamics across a heterogeneous toughness landscape.** (A) Fracture fronts (black lines) obtained by sampling a solution of Eqs. (4) at intervals $\Delta t = 1.72$. Colors indicate the local toughness contrast $D\eta$. A section of the periodic xz fracture plane is shown. Inset: geometry of the full fracture plane. The main panel section is highlighted in blue. $L_x = 1552, L_z = 257.8$ and $\Delta z = 0.1$. (B) A section of the fracture plane corresponding to the dashed red rectangle in (A). Fronts are $\Delta t = 0.431$ apart. (C) The local velocity fluctuation of the fronts depicted in (B) is plotted as a function of $x = Vt$ and z . Red dashed lines represent the predicted front wave directions. Solution parameters: $\nu = 0.3, V = 0.5c_R, D = 0.2, \psi = 0.5$.

Fisher [13] obtained

$$\widehat{\delta G} = -2|k|P_1(\omega/|k|; V, \nu)\hat{f} + \mathcal{O}(f^2), \quad (2)$$

where ν is the Poisson ratio and P_1 is an explicit function of its arguments [43]. Through Eq. (1), the kernel $-2|k|P_1$ defines the linear response of the crack front to spatial variations in Γ . Particularly, $P_1(\omega/|k| = s_{FW}) = 0$ for $s_{FW} \equiv \xi(V/c_R, \nu)\sqrt{c_R^2 - V^2}$, where c_R is the Rayleigh wave speed and ξ is a factor very close to, but smaller, than 1. Thus, crack fronts support one-dimensional dispersion-less wave propagation, whose existence was corroborated numerically and experimentally [38, 40–42]. The total dissipation, however, remains unchanged in the 1st-order.

To determine how moderate heterogeneity affects dissipation in dynamic fracture, we extended the perturbation theory to the 2nd-order in f . The three-dimensional elastodynamic fields were analytically resolved close to the crack front and the energy release rate was computed through a self-consistent expansion [33]. This calculation resulted in the perturbation expansion $\widehat{\delta G} = \widehat{\delta G}_1[\hat{f}] + \widehat{\delta G}_2[\hat{f}, \hat{f}] + \mathcal{O}(f^3)$, in which the linear part $\widehat{\delta G}_1$ is given by Eq. (2), and the 2nd-order contribution is

$$\begin{aligned} \widehat{\delta G}_2 &= 2|k|P_1\{\hat{f} * |k|P_1\hat{f}\} - \frac{1}{2}\{k^2P_1^2 + iV\omega|k|P_2\}\hat{f} * \hat{f} \\ &- \hat{f} * (k^2P_1^2 - iV\omega|k|P_2)\hat{f} + |k|P_1\hat{f} * |k|P_1\hat{f} \end{aligned} \quad (3)$$

where $P_2 = P_2(\omega/|k|; V, \nu)$ is an explicit function of its arguments [33], and the convolution is $(f * g)(k, \omega) =$

$(2\pi)^{-2} \int dk' d\omega' f(k - k', \omega - \omega')g(k', \omega')$. Eq. (3) reproduced known expressions at the limits of $k \rightarrow 0$ and $\omega \rightarrow 0$ and was shown to agree with the history-dependent form $G(z, t) = G_r g(V_\perp)(1 + H[f(z', t' \leq t)])$ [13, 33, 43]. To determine the time evolution of the front in the presence of heterogeneity, we modeled the fracture energy as a product $\Gamma = \Gamma_0(V_\perp)(1 + D\eta(z, x))$ of a velocity-dependent part $\Gamma_0(V) = 1 + \psi V$, and a fluctuating part. The heterogeneity landscape η was a Gaussian random field of zero mean and unit variance. The definition of Γ_0 entailed an implicit choice of the energy units. Energy balance, then, required that $\delta G = \delta \Gamma$, where $\delta \Gamma \equiv \Gamma/\Gamma_0(V) - 1$. To proceed, we expanded $f = Df_1 + D^2f_2 + \mathcal{O}(D^3)$ and solved the perturbation hierarchy in Fourier space,

$$\hat{f}_1 = C_{ff}\hat{\eta}; \quad \hat{f}_2 = C_{ff}(\widehat{\delta \Gamma}_2 - \widehat{\delta G}_2[\hat{f}_1, \hat{f}_1]), \quad (4)$$

where $C_{ff} = -(2|k|P_1 + i\omega\psi)^{-1}$, except at $(k = 0, \omega = 0)$ where $C_{ff} = 0$, and $\delta \Gamma_2 = f_1\partial_x\eta + \psi\eta\partial_t f_1 - \psi\frac{V}{2}(\partial_z f_1)^2$.

To gain insight, we numerically evaluated Eqs. (4) on a periodic rectangle (L_x, L_z) for an exponentially correlated heterogeneity field $\langle \eta(z, x)\eta(z', x') \rangle = C(\sqrt{(z - z')^2 + (x - x')^2})$ where $C(r) = e^{-r/\ell}$. The units of time and space were chosen such that the shear wave speed $c_s = 1$ and $\ell = 1$. The fracture energy heterogeneity gave rise to spatiotemporal crack front fluctuations (Fig. 1A, Supplementary Video 1). Regions of increased (decreased) toughness locally slowed down (accelerated) the crack front (Fig. 1B). For weakly velocity-dependent Γ_0 , the local velocity fluctuation $D\partial_t f_1 + D^2\partial_t f_2$ exhibited oblique patterns across the fracture

plane (Fig. 1C). The slopes predicted for crack front waves, $\pm s_{FW}/\sqrt{s_{FW}^2 + V^2}$, approximated those of the velocity patterns.

The heterogeneous landscape excited in-plane front roughness. To quantify the roughness, we calculated the static structure factor (SSF) of the crack front $S(k) = \int d\omega |\hat{f}(k, \omega)|^2$. The SSF decayed for all k . For small amplitude heterogeneity, $S(k)$ approximately followed a k^{-1} decay until $k \sim 0.5$ where it crossed-over to a k^{-4} decay. These scaling relations were confirmed by an analytical calculation [43]. At higher D values and weak velocity-dependence $\psi \ll 1$, the SSF decay at short wavelengths weakened (Fig. 2A). Thus, the crack fronts in this regime are populated by small-scale roughness that is not present in the linear solution. For strong velocity-dependence ($\psi \gg 1$), the SSF shape was approximately unchanged as D was increased (Fig. 2B). When $S(k) \sim k^{-\alpha}$, the scaling exponent α is related to the roughness exponent ζ defined by $\sqrt{\langle (f(z + \Delta z) - f(z))^2 \rangle} \sim \Delta z^\zeta$ via the equation $\alpha = 1 + 2\zeta$. Accordingly, our calculations are consistent with $\zeta \sim 0$ when $D < 0.1$ or $\psi > 1$. For $\psi \ll 1$, we identify this exponent with the logarithmic in-plane roughness associated with front waves [44]. For $\psi \ll 1$ and $D \sim 0.2$, the SSF roughly follows a $\alpha \sim 1.3$ scaling which corresponds to $\zeta \sim 0.15$. The SSF decay is then much weaker than that observed in quasi-static fracture experiments [45], indicating a fundamental difference with dynamic cracks.

Front fluctuations renormalize dissipation. To investigate how the 2nd-order corrections, δG_2 and $\delta \Gamma_2$, modify the overall dissipation, we re-examined the local energy balance, Eq. (1). The substitution of the perturbative solution (Eqs. (4)) in the 2nd-order expressions for G and Γ showed that $\langle \delta G - \delta \Gamma \rangle \sim \mathcal{O}(D^2)$, where $\langle \rangle$ denotes ensemble averaging over realizations of η . Energy balance appeared, then, to be globally violated. The origin of this apparent contradiction is the decomposition of f into periodic functions over the rectangle ($L_z, L_x/V$), which precludes global changes to the

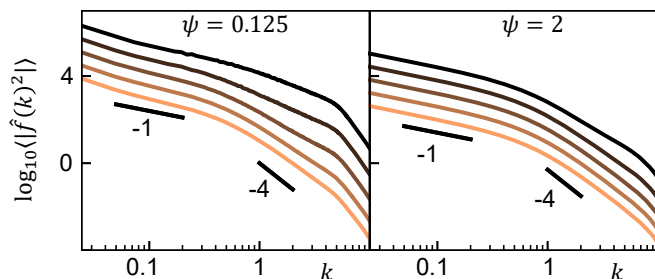


FIG. 2. **Static structure factors of the crack front fluctuations.** Colors correspond to $D = 0.0125$ (light), 0.025, 0.05, 0.1, 0.2 (dark). Curves averaged over 10 realizations of η . Black lines and adjacent numbers depict the slopes of power-law curves. $\nu = 0.3$, $V = 0.5c_R$, $L_z = 257.8$, $L_x = 1552$, $\Delta z = 0.1$.

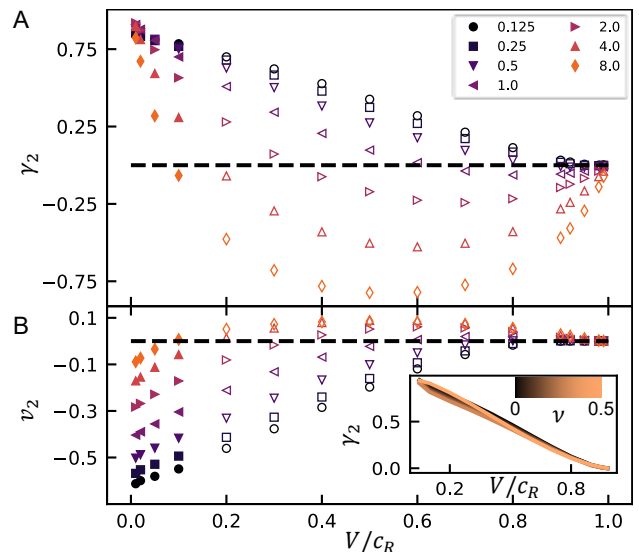


FIG. 3. **Renormalization prefactors** for (A) the fracture energy and (B) the crack velocity. $L_z = 75.2$, $L_x = 5330.65$ (full symbols), $L_z = 1386.4$, $L_x = 288.526$ (empty symbols). Inset: Variation of γ_2 with the Poisson ratio ν . $\psi = 0.125$, $L_z = 75.2$, $L_x = 5330.65$.

crack velocity. To recover energy balance, we add a constant velocity term by writing $f = \delta V t + f_r$ where $\langle f_r \rangle = 0$ and $\delta V \sim \mathcal{O}(D^2)$. Eqs. (4), therefore, hold for $f_r = Df_1 + D^2f_2 + \mathcal{O}(D^3)$. The renormalized crack velocity is $V + \delta V = V + v_2D^2 + \mathcal{O}(D^3)$, where $v_2 = \frac{1}{\psi + 2\pi_1} \{ \langle (k^2(|P_1|^2 - P_1^2) + iV\omega|k|P_2)|\hat{f}_1|^2) - \gamma_2 \}$ and $\pi_1 = \lim_{k \rightarrow 0} |k|P_1(\omega/|k|)/(i\omega)$ [33]. The renormalization coefficient $\gamma_2 = \langle f_1 \partial_x \eta + \psi \eta \partial_t f_1 - \psi \frac{V}{2} (\partial_z f_1)^2 \rangle$ tunes the global dissipation via $\langle \Gamma \rangle = \Gamma_0(V)(1 + \gamma_2 D^2) + \mathcal{O}(D^3)$. The sign of v_2 determines whether heterogeneity assists or hinders fracture.

What are the consequences of heterogeneity to the overall dissipation? To find out, we computed γ_2 using an analytical integral, Eq. (S5), that was numerically evaluated over the discretized Fourier domain ($k_{max} = \pi/\Delta z$, $\omega_{max} = \pi V/\Delta z$) where Δz is the real space discretization and $\Delta k = 2\pi/L_z$, $\Delta \omega = 2\pi V/L_x$. The fracture plane (L_x, L_z) was made sufficiently large to obtain approximately size-independent results. For $\psi \ll 1$, the dissipation renormalization prefactor was positive and decreased with crack velocity (Fig. 3A). Calculations for a range of Poisson ratios $0 \leq \nu \leq 0.5$ showed that γ_2 depends on the material elasticity almost exclusively through the ratio of V to the Rayleigh wave speed c_R (Fig. 3A inset). At the two limiting velocities, $V \rightarrow 0$ and $V \rightarrow c_R$, γ_2 approached ψ -independent limits. Upon increasing ψ , γ_2 decreased and attained negative values in a widening range of V . Thus, heterogeneity is predicted to increase dissipation in materials whose toughness is weakly velocity-dependent. In strongly velocity-dependent materials, however, dissipation is predicted to

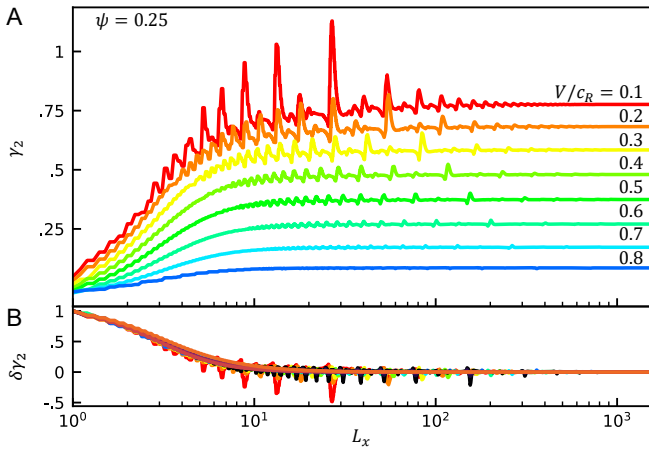


FIG. 4. **Finite size effect.** (A) The fracture energy prefactor increases with system length. (B) Collapse of curves in (A) and Fig. S2 by $\delta\gamma_2 = (\gamma_2(L_x) - \gamma_2(1551))/(\gamma_2(1) - \gamma_2(1551))$. $\nu = 0.3$, $L_z = 257.8$, $\Delta z = 0.1$.

decrease above a ψ -dependent velocity.

The renormalization of dissipation was associated with a renormalization of crack velocity. The coefficient v_2 was negative for $\psi \ll 1$ (Fig. 3B). For larger values of ψ , v_2 increased and attained positive values over a broad crack velocity range. At limiting velocities, v_2 approached a vanishing ψ -independent limit at $V \rightarrow c_R$ and a ψ -dependent value at $V \rightarrow 0$. To estimate the interval $0 < D < \tilde{D}$ in which $\delta V \simeq v_2 D^2$ is the leading correction to the global crack velocity, we approximated $\tilde{D} \simeq \sqrt{\langle f_1^2 \rangle / \langle f_2^2 \rangle}$, where f_1, f_2 are defined in Eqs. (4). In the range of velocities $0.1c_R < V < 0.9c_R$, the interval limit was $\tilde{D} \sim 20\%$ for $\psi \ll 1$, and increased to $\tilde{D} \gtrsim 100\%$ when $\psi \gg 1$ (Fig. S1). These results indicate that the 2nd-order approximation applies to a wide range of heterogeneity fields, materials, and loading conditions.

The renormalized dissipation exhibited finite-size dependence. To investigate, we numerically computed $\gamma_2(L_x; V, \psi)$ for a fixed L_z . $\gamma_2(L_x)$ increased monotonically with $L_x < 10\ell$ where ℓ is the heterogeneity correlation length (Fig. 4A, Fig. S2). At $L_x \sim 10\ell$, γ_2 approached an asymptotic size-independent value. Through a linear transformation, all the functions $\gamma_2(L_x; V, \psi)$ approximately collapsed on a single master curve, showing that the asymptotic length scale $L_x \sim 10\ell$ was independent of V and ψ (Fig. 4B). The manner of the asymptotic approach, however, changed with the parameters. For $\psi \geq 1$, γ_2 approached the asymptote smoothly, without appreciable deviations from it for $L_x > 20\ell$. For $\psi \ll 1$, γ_2 approached the asymptote while exhibiting spike-like fluctuations that persisted until $L_x > 10^3$. The amplitudes of the isolated spikes increased inversely with the crack velocity. Since γ_2 was evaluated through Eq. (S5), where ensemble averaging is analytically performed, there is no stochastic component that could give

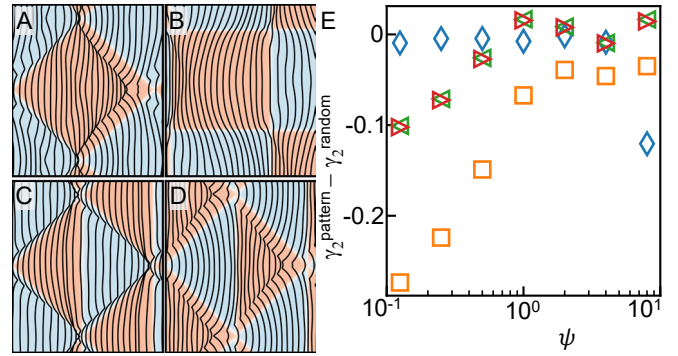


FIG. 5. **Renormalized dissipation of patterned planes.** Crack fronts overlay (black lines) (Eq. (4)) on the toughness patterns (colors): (A) checkered diamonds, (B) checkered squares, (C) left-pointing and (D) right-pointing triangles. Colors denote $\eta = 1.2$ (light red) $\eta = -0.92$ (light blue). Side of a square in (B), 20. Time interval between crack fronts, 1.742. $\psi = 0.5$. $D = 0.2$ (E) Differences between γ_2 values for the patterns (A-D) and the random exponentially-correlated field. System size, $L_z = 257.8$, $L_x = 1552$. All panels, $V = 0.5c_R$, $\nu = 0.3$, $\Delta z = 0.1$.

rise to fluctuations. Instead, the finite-size spikes are expected to arise from front wave propagation in a finite geometry.

What is the origin of the renormalization of dissipation by heterogeneity? The fracture energy Γ contains asymmetric 2nd-order contributions that arise from the coupling of front dynamics to the toughness landscape. The first contribution to the renormalization coefficient γ_2 couples the front position to gradients of the heterogeneity field. This effect is the dynamic version of the weak pinning observed in quasi-static cracks [46]. In the limit $L_x, L_z \rightarrow \infty$, this term may be written as $\langle f_1 \partial_x \eta \rangle = (L_x L_z)^{-1} \int dz (f_1 \eta|_{x=L_x} - f_1 \eta|_{x=0}) - (L_x L_z)^{-1} \int dt dz \eta \partial_t f_1$. The boundary terms vanishes as L_x^{-1} when $L_x \rightarrow \infty$. The second integral is positive since locally increased toughness $\eta > 0$ retard the front $\partial_t f < 0$. The second contribution $\psi \langle \eta \partial_t f_1 \rangle$ is negative by the same argument. The third contribution $-\frac{1}{2} \psi V \langle (\partial_z f_1)^2 \rangle$, that results from front propagation along the local normal, is negative definite. Thus, velocity dependence of the fracture energy acts to reduce toughness. The competition between terms of opposite signs results in a dual effect which is confirmed by an analytical calculation (Eq. (S5)). All terms vanish as $V \rightarrow c_R$ because higher crack inertia lessens the retardance of the front by asperities. This is a possible explanation for the decrease of fracture energy with velocity in glass [34].

Control of dynamic fracture by patterning. Our semi-analytical framework can be used to probe the influence of toughness design on crack propagation. To shed light, we solved Eq. (1) for four periodic patterns with $\langle \eta \rangle = 0$ and $\langle \eta^2 \rangle = 1$ (Fig. 5A-D, Supplementary Videos 2-5).

Two of them, checkered diamonds and squares, were symmetric to the crack propagation direction. The two other patterns were mirror images of an asymmetric triangular pattern. In the diamond and triangular cases, the crack fronts exhibited large spatial and temporal gradients, whereas deformations were relatively small in the case of the squares pattern. To find how γ_2 depend on design, we quantified their deviations from the γ_2 values for random heterogeneity (Fig. 5E). The diamond pattern produced similar γ_2 values except for large ψ . The checkerboard pattern, however, exhibited much reduced γ_2 . Surprisingly, front propagation through the two asymmetric triangular patterns resulted in approximately identical γ_2 . These results indicate that, unlike quasi-static cracks, dynamic fracture may be insensitive to pattern asymmetry. In contrast, since the diamond and square patterns are related by a 45° rotation, symmetric patterning may be used to create “hard” and “easy” directions for crack propagation.

Discussion. Our study leaves the question of transients open. To encompass such events, G may be transformed into the time domain [33]. In heterogeneous media with $\psi = 0$, front fluctuations grow linearly in time [15]. An inspection of C_{ff} reveals that, for $0 < \psi \ll 1$, fronts should approach steady state at $t \sim |P'_1(s_{FW})|(\pi s_{FW}\psi)^{-1}L_z$, the lifetime of the longest front wave. However, local front arrests, $G(z, t) < \Gamma(z, t)$, may modify the steady-state predictions.

The dominance of front waves when $\psi \ll 1$ raises questions about nonlinear wave-wave interactions. Since $P_2(s_{FW}) \neq 0$ [33] waves have a non-zero contribution to G at the 2nd-order. Resonant wave interactions may then contribute to G in the 1st-order in D and populate small wavelengths in the SSF (Fig. 2A). How would the interactions translate into dissipation is an open question.

How do the predictions change for finite-size bodies [47, 48], besides the size effect described in Fig. 4? In strip-like geometries, where $L_x, L_z \ll L_y$ the supplied energy per unit crack length is a constant [49]. The integral dissipation $\int dl_c \Gamma(z, t; V_\perp)$ over the front contour $l_c(t)$ is therefore fixed by the loading [16]. Crack front fluctuations will increase l_c , resulting in decreased velocities. Loading at a finite distance b from the crack tip adds $\mathcal{O}(\|f\|/b)$ terms in G , which give rise to front wave dispersion [33, 38].

Cracks in heterogeneous materials often produce rough surfaces whose excess area increases the local dissipation. By projecting the dissipation to a plane, $\Gamma(x, z)$, Eq. (1) can be used to predict the in-plane front dynamics. Such a methodology may open a way to predict the propagation of rough fractures at realistic scales.

The authors acknowledge enlightening discussions with the participants of the CECAM flagship workshop 3D cracks and crack stability (June 2023, Lausanne). I.K. is grateful for fruitful conversations with Sharad Ramanathan and Shmuel Rubinstein.

* ikolvin@gatech.edu

- [1] J. D. Bedford, D. R. Faulkner, and N. Lapusta, Fault rock heterogeneity can produce fault weakness and reduce fault stability, *Nature Communications* **13**, 326 (2022).
- [2] S. Ray and R. C. Viesca, Earthquake Nucleation on Faults With Heterogeneous Frictional Properties, Normal Stress, *Journal of Geophysical Research: Solid Earth* **122**, 8214 (2017).
- [3] T. Taufiqurrahman, A.-A. Gabriel, D. Li, T. Ulrich, B. Li, S. Carena, A. Verdecchia, and F. Gallovič, Dynamics, interactions and delays of the 2019 Ridgecrest rupture sequence, *Nature* **618**, 308 (2023).
- [4] A. Gouyon, S. Latour, J. Letort, and S. El Arem, Rupture Nucleation on a Periodically Heterogeneous Interface, *Geophysical Research Letters* **49**, e2021GL096816 (2022).
- [5] Y. Faure and E. Bayart, Experimental evidence of seismic ruptures initiated by aseismic slip (2023), arXiv:2312.17511 [cond-mat, physics:physics].
- [6] D. I. Garagash, Fracture mechanics of rate-and-state faults and fluid injection induced slip, *Philosophical Transactions of the Royal Society A: Mathematical, Physical and Engineering Sciences* **379**, 20200129 (2021).
- [7] F. Barthelat, The Fracture Mechanics of Biological Materials, in *Mechanics and Physics of Fracture: Multi-scale Modeling of the Failure Behavior of Solids*, edited by L. Ponson (Springer International Publishing, Cham, 2023) pp. 255–282.
- [8] A. Amini, A. Khavari, F. Barthelat, and A. J. Ehrlicher, Centrifugation and index matching yield a strong and transparent bioinspired nacreous composite, *Science* **373**, 1229 (2021).
- [9] A. J. D. Shaikkea, H. Cui, M. O’Masta, X. R. Zheng, and V. S. Deshpande, The toughness of mechanical metamaterials, *Nature Materials* **21**, 297 (2022).
- [10] S. Gupta, H. S. Esmaeeli, and R. Moini, Tough and Ductile Architected Nacre-Like Cementitious Composites, *Advanced Functional Materials* **n/a**, 2313516.
- [11] Z. Hashin, The Elastic Moduli of Heterogeneous Materials, *Journal of Applied Mechanics* **29**, 143 (1962).
- [12] J. R. Willis and A. B. Movchan, Dynamic weight functions for a moving crack. I. Mode I loading, *Journal of the Mechanics and Physics of Solids* **43**, 319 (1995).
- [13] S. Ramanathan and D. S. Fisher, Dynamics and instabilities of planar tensile cracks in heterogeneous media, *Physical Review Letters* **79**, 877 (1997).
- [14] A. B. Movchan, H. Gao, and J. R. Willis, On perturbations of plane cracks, *International Journal of Solids and Structures* **35**, 3419 (1998).
- [15] J. W. Morrissey and J. R. Rice, Perturbative simulations of crack front waves, *Journal of the Mechanics and Physics of Solids* **48**, 1229 (2000).
- [16] M. Wang, M. Adda-Bedia, J. M. Kolinski, and J. Fineberg, How hidden 3D structure within crack fronts reveals energy balance, *Journal of the Mechanics and Physics of Solids* **161**, 104795 (2022).
- [17] X. Wei, C. Li, C. McCarthy, and J. M. Kolinski, Complexity of crack front geometry enhances toughness of brittle solids, *Nature Physics*, 1 (2024).
- [18] A. Sanner, N. Kumar, A. Dhinojwala, T. D. B. Jacobs, and L. Pastewka, Why soft contacts are stickier when

- breaking than when making them, *Science Advances* **10**, ead11277 (2024).
- [19] V. Démery, A. Rosso, and L. Ponson, From microstructural features to effective toughness in disordered brittle solids, *EPL (Europhysics Letters)* **105**, 34003 (2014).
- [20] J. Chopin, A. Bhaskar, A. Jog, and L. Ponson, Depinning Dynamics of Crack Fronts, *Physical Review Letters* **121**, 235501 (2018).
- [21] G. Albertini, M. Lebihain, F. Hild, L. Ponson, and D. S. Kammer, Effective Toughness of Heterogeneous Materials with Rate-Dependent Fracture Energy, *Physical Review Letters* **127**, 035501 (2021).
- [22] K. H. Pham and K. Ravi-Chandar, On the growth of cracks under mixed-mode I+ III loading, *International Journal of Fracture* **199**, 105 (2016).
- [23] W. Steinhardt and S. M. Rubinstein, How Material Heterogeneity Creates Rough Fractures, *Physical Review Letters* **129**, 128001 (2022).
- [24] M. Lebihain, J.-B. Leblond, and L. Ponson, Effective toughness of periodic heterogeneous materials: The effect of out-of-plane excursions of cracks, *Journal of the Mechanics and Physics of Solids* **137**, 103876 (2020).
- [25] Y. Lubomirsky and E. Bouchbinder, Quenched disorder and instability control dynamic fracture in three dimensions (2023), arXiv:2311.11692 [cond-mat, physics:nlin].
- [26] E. Sharon, S. P. Gross, and J. Fineberg, Energy Dissipation in Dynamic Fracture, *Physical Review Letters* **76**, 2117 (1996).
- [27] T. Roch, M. Lebihain, and J.-F. Molinari, Dynamic Crack-Front Deformations in Cohesive Materials, *Physical Review Letters* **131**, 096101 (2023).
- [28] A. J. Pons and A. Karma, Helical crack-front instability in mixed-mode fracture, *Nature* **464**, 85 (2010).
- [29] H. Henry and M. Adda-Bedia, Fractographic aspects of crack branching instability using a phase-field model, *Physical Review E* **88**, 060401 (2013).
- [30] C.-H. Chen, T. Cambonie, V. Lazarus, M. Nicoli, A. J. Pons, and A. Karma, Crack front segmentation and facet coarsening in mixed-mode fracture, *Physical review letters* **115**, 265503 (2015).
- [31] J. J. Möller and E. Bitzek, On the influence of crack front curvature on the fracture behavior of nanoscale cracks, *Engineering Fracture Mechanics* **150**, 197 (2015).
- [32] M. J. Buehler, Modeling Atomistic Dynamic Fracture Mechanisms Using a Progressive Transformer Diffusion Model, *Journal of Applied Mechanics* **89**, 10.1115/1.4055730 (2022).
- [33] I. Kolvin and M. Adda-Bedia, A comprehensive study of nonlinear perturbations in the dynamics of planar crack fronts (2024), arXiv:2404.18633 [cond-mat, physics:physics].
- [34] E. Sharon and J. Fineberg, Confirming the continuum theory of dynamic brittle fracture for fast cracks, *Nature* **397**, 333 (1999).
- [35] J. A. Hauch, D. Holland, M. P. Marder, and H. L. Swinney, Dynamic fracture in single crystal silicon, *Physical Review Letters* **82**, 3823 (1999).
- [36] T. Baumberger, C. Caroli, and D. Martina, Solvent control of crack dynamics in a reversible hydrogel., *Nature Materials* **5** (2006).
- [37] L. B. Freund, *Dynamic Fracture Mechanics* (Cambridge University Press, Cambridge; New York, 1990).
- [38] A. N. Norris and I. D. Abrahams, A multiple-scales approach to crack-front waves, *Journal of Engineering Mathematics* **59**, 399 (2007).
- [39] M. Adda-Bedia, R. E. Arias, E. Bouchbinder, and E. Katzav, Dynamic Stability of Crack Fronts: Out-Of-Plane Corrugations, *Physical Review Letters* **110**, 014302 (2013).
- [40] E. Sharon, G. Cohen, and J. Fineberg, Propagating solitary waves along a rapidly moving crack front, *Nature* **410**, 68 (2001).
- [41] F. Fekak, F. Barras, A. Dubois, D. Spielmann, D. Bonamy, P. H. Geubelle, and J. F. Molinari, Crack front waves: A 3D dynamic response to a local perturbation of tensile and shear cracks, *Journal of the Mechanics and Physics of Solids* **135**, 103806 (2020).
- [42] S. Das, Y. Lubomirsky, and E. Bouchbinder, Dynamics of crack front waves in three-dimensional material failure, *Physical Review E* **108**, L043002 (2023).
- [43] I. Kolvin and M. Adda-Bedia, Supplemental Material for "Dual role for heterogeneity in dynamic fracture".
- [44] E. Bouchaud, JP. Bouchaud, DS. Fisher, S. Ramanathan, and JR. Rice, Can crack front waves explain the roughness of cracks?, *Journal of the Mechanics and Physics of Solids* **50**, 1703 (2002).
- [45] J. Schmittbuhl and K. J. Måløy, Direct Observation of a Self-Affine Crack Propagation, *Physical Review Letters* **78**, 3888 (1997).
- [46] D. Dalmas, E. Barthel, and D. Vandembroucq, Crack front pinning by design in planar heterogeneous interfaces, *Journal of the Mechanics and Physics of Solids* **57**, 446 (2009).
- [47] N. Xue, R. Long, E. R. Dufresne, and R. W. Style, Elastomers Fail from the Edge, *Physical Review X* **14**, 011054 (2024).
- [48] Z. P. Bazant and P. A. Pfeiffer, Determination of Fracture Energy from Size Effect and Brittleness Number, *Materials Journal* **84**, 463 (1987).
- [49] T. Goldman, A. Livne, and J. Fineberg, Acquisition of Inertia by a Moving Crack, *Physical Review Letters* **104**, 114301 (2010).

Supplementary Material for “Dual Role for Heterogeneity in Dynamic Fracture”

Itamar Kolvin*

School of Physics, Georgia Institute of Technology, 837 State St NW, Atlanta, 30332, GA, USA

Mokhtar Adda-Bedia

Laboratoire de Physique, CNRS, ENS de Lyon, Université de Lyon, F-69364 Lyon, France

(Dated: July 3, 2024)

EXPLICIT EXPRESSIONS FOR THE KERNELS P_1 AND P_2

In a separate manuscript, we derived explicit expressions for $\widehat{\delta G}_1$ and $\widehat{\delta G}_2$ of the stress and displacement fields surrounding the crack front [1]. The kernels, $P_1(\omega/|k|; V)$ and $P_2(\omega/|k|; V)$, that appear in the main text are

$$P_1(s; V) = -\frac{1}{2}\gamma_l \sqrt{1 - \frac{\gamma_l^2 s^2}{c_l^2}} + \gamma_R \sqrt{1 - \frac{\gamma_R^2 s^2}{c_R^2}} + \frac{1}{2} \int_{c_s}^{c_l} \frac{(s^2 + V^2)(\eta^2 + V^2) - 2\eta^2 V^2}{\sqrt{\eta^2 - (s^2 + V^2)}(\eta^2 - V^2)^2} \Theta(\eta) d\eta, \quad (S1)$$

and

$$P_2(s; V) = 2\frac{\gamma_R^3}{c_R^2} \sqrt{1 - \frac{\gamma_R^2 s^2}{c_R^2}} - \frac{\gamma_l^3}{c_l^2} \sqrt{1 - \frac{\gamma_l^2 s^2}{c_l^2}} + \int_{c_s}^{c_l} \frac{(s^2 + V^2)(3\eta^2 + V^2) - 2\eta^2(\eta^2 + V^2)}{\sqrt{\eta^2 - (s^2 + V^2)}(\eta^2 - V^2)^3} \Theta(\eta) d\eta, \quad (S2)$$

where $\gamma_l = 1/\sqrt{1 - V^2/c_l^2}$; $\gamma_R = 1/\sqrt{1 - V^2/c_R^2}$; and

$$\Theta(\eta) = \frac{2}{\pi} \arctan \left[4\sqrt{1 - \frac{\eta^2}{c_l^2}} \sqrt{\frac{\eta^2}{c_s^2} - 1} / \left(2 - \frac{\eta^2}{c_s^2}\right)^2 \right].$$

c_l and c_s are the longitudinal and shear wave speeds respectively. The branch cuts of the square roots are defined such that $\sqrt{1 - s^2} = i \operatorname{sign}(s) \sqrt{s^2 - 1}$ for $|s| > 1$.

Recovery of known limits for $k \rightarrow 0$ and $\omega \rightarrow 0$. To test the validity of Eq. (3) in the main text, we compare it to known expressions for simple or quasi-static crack fronts. In the simple crack limit, $|k| \rightarrow 0$ and $|k|P_1 \rightarrow -i\omega\pi_1$; $|k|P_2 \rightarrow -i\omega\pi_2$ where

$$\pi_1 = \frac{1}{2} \frac{c_l}{c_l^2 - V^2} - \frac{c_R}{c_R^2 - V^2} + \frac{1}{2} \int_{c_s}^{c_l} \frac{\eta^2 + V^2}{(\eta^2 - V^2)^2} \Theta(\eta) d\eta, \quad (S3)$$

and

$$\pi_2 = \frac{c_l}{(c_l^2 - V^2)^2} - 2\frac{c_R}{(c_R^2 - V^2)^2} + \int_{c_s}^{c_l} \frac{3\eta^2 + V^2}{(\eta^2 - V^2)^3} \Theta(\eta) d\eta. \quad (S4)$$

As a result, Eq. (3) approaches the limit $\widehat{\delta G}_2 \rightarrow -(2\pi_1^2 + V\pi_2)(\omega f) * (\omega f)$, which translates into the real space expression

$$\delta G_2 = (2\pi_1^2 + V\pi_2)f'(t)^2. \quad (S5)$$

To compare with the known expression for simple cracks [2], the 2D energy release rate is expanded $G = G_r g(V + f'(t)) \simeq G_r (g(V) + g'(V)f'(t) + g''(V)f'(t)^2/2)$. The 2nd-order correction is therefore $\delta G_2 = \frac{g''(V)}{2g(V)} f'(t)^2$. From Chapter 6 in [2] one may prove the identity $\pi_1 = \frac{g'(V)}{2g(V)}$. As a corollary, $\frac{g''(V)}{2g(V)} = 2\pi_1^2 + \pi_1'(V)$. From Eqs. (S3-S4), it is straightforward to show that $\pi_1'(V) = V\pi_2$ by differentiation and Eq. (S5) is reproduced.

In the quasi-static limit, $\omega \rightarrow 0$ and $V \rightarrow 0$. Eq. (3) becomes

$$\delta G_2 = \frac{1}{4} \int dk' f(k - k') f(k') \{ |k| (|k'| + |k - k'|) - k^2 + k'(k - k') + |k'| |k - k'| \}.$$

The same expression is obtained from the static 2nd-order approximation of the stress intensity factor [3].

ANALYTICAL EXPRESSIONS FOR THE SSF, γ_2 AND v_2

One can approximate C_{ff} as follows. For $\psi \ll 1$, $C_{ff} \simeq [\mp 2|k|P_1'(s_{FW})(\omega/|k| \mp s_{FW}) - i\psi\omega]^{-1}$ where the sign is $-$ or $+$ for $\omega > 0$ and $\omega < 0$ respectively. When $\psi \gg 1$, $C_{ff} \simeq -(2|k|P_1(0) + i\psi\omega)^{-1}$.

Using these approximations we calculate the static structure factor of f_1 . From $\hat{f}_1 = C_{ff}\hat{\eta}$ we find that $\langle |f_1(k, t)|^2 \rangle \simeq (\pi V)^{-1} \int_0^\infty d\omega |C_{ff}|^2 S(p)$ where $p = \sqrt{k^2 + (\omega/V)^2}$. Applying the approximations for $\psi \ll 1$

$$\langle |f_1(k, t)|^2 \rangle \simeq \frac{1}{V\psi P_1'(s_{FW})s_{FW}} \frac{S(k\sqrt{1 + (s_{FW}/V)^2})}{|k|}$$

and for $\psi \gg 1$

$$\langle |f_1(k, t)|^2 \rangle \simeq \frac{1}{4V\psi P_1(0)} \frac{S(k)}{|k|}$$

Similarly,

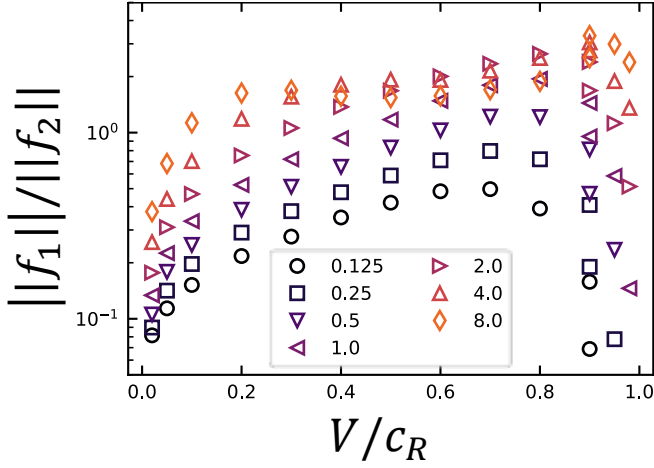


FIG. S1. The ratio of the norms of the 1st-order and the 2nd-order corrections to the crack front dynamics (Eqs. (3)). System size, $L_z = 75.2$, $L_x = 5330.65$. All panels, symbols, and colors indicate ψ values, $\nu = 0.3$, $\Delta z = 0.1$.

$$\gamma_2 = \int_0^\infty dk \int_0^\infty d\omega \frac{S(p)}{\pi^2} \left[\frac{1 - \psi V}{V^2} \omega \Im C_{ff} - \frac{\psi}{2} k^2 |C_{ff}|^2 \right] \quad (S6)$$

and

$$v_2 = \frac{1}{\psi + 2\pi_1} \left(\int_0^\infty dk \int_0^\infty d\omega \frac{S(p)}{\pi^2} [k^2 (|P_1(s)|^2 - P_1(s)^2) + iV\omega k P_2(s)] |C_{ff}|^2 - \gamma_2 \right) \quad (S7)$$

where $s = \omega/k$. To evaluate the integrals in Eqs. (S6-S7), the (k, ω) space was discretized at steps of size $\Delta k = 2\pi/L_z$ and $\Delta\omega = 2\pi V/L_x$ and the maximum wavelength was $k_{max} = \pi/\Delta z$ and the maximum frequency was $\omega_{max} = \pi V/\Delta z$. The integrals were then computed in NumPy using a trapezoidal approximation. Note that $\Im C_{ff}$ is non-negative, which means that γ_2 takes positive values for $\psi \ll 1$, and may become negative for large enough ψ .

CONSTRUCTION OF THE RANDOM HETEROGENEITY FIELD $\eta(z, x)$

In the main text, $\eta(z, x)$ defines the fluctuation of the heterogeneous fracture energy across the fracture plane. We construct η as a Gaussian random field with zero mean and covariance $\langle \eta(z, x)\eta(z', x') \rangle = C(\sqrt{(x-x')^2 + (z-z')^2})$ where $C(r) = e^{-r/\ell}$ with ℓ , the correlation length. The corresponding structure factor is $S(\sqrt{k^2 + q^2}) = \int dx dz e^{-ikz - iqx} C(\sqrt{x^2 + z^2})$, or,

$$S(p) = \frac{2\pi\ell^2}{(1 + p^2\ell^2)^{3/2}}. \quad (S8)$$

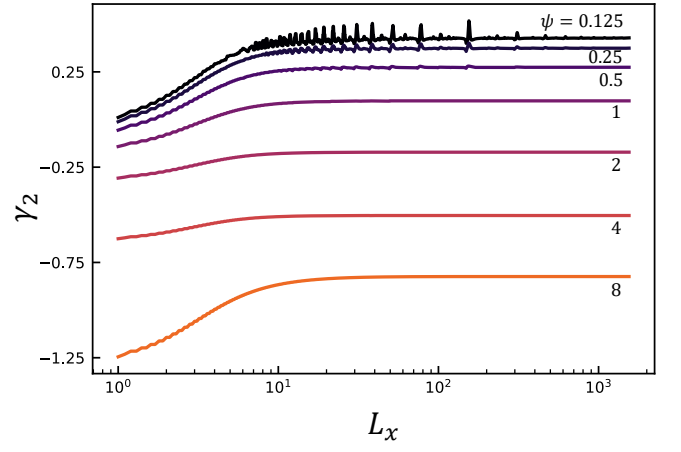


FIG. S2. Collapse of all curves in (A) and (B) by normalizing $\delta\gamma_2 = (\gamma_2(L_x) - \gamma_2(1551))/(\gamma_2(1) - \gamma_2(1551))$. Solution parameters, $\nu = 0.3$, $L_z = 257.8$, $\Delta z = 0.1$.

To numerically generate η , the (k, ω) plane is discretized as $k_n = 2\pi n/L_z$ and $\omega_m = 2\pi m V/L_x$, with the Nyquist limits $k_{N_z/2} = \pi/\Delta z$ and $\omega_{N_x/2} = \pi V/\Delta z$. The discrete heterogeneity field is then $\hat{\eta}_{nm} = e^{i\phi_{nm}} \sqrt{S_{nm}}/V$ where ϕ_{nm} are random variables that are sampled from a uniform distribution in the $[0, 2\pi)$ interval. To obtain smoothly varying fields, we add a high wave-number cutoff, $S_{nm} \propto S(p_{nm})/\sqrt{1 + (p_{nm}\Delta z)^2}$ where $p_{nm}^2 = k_n^2 + (\omega_m/V)^2$. The components S_{nm} are normalized to obtain an η field of unit variance.

Supplementary Video 1 Crack fronts propagating in a heterogeneous toughness landscape. Fronts shown at time intervals $\Delta t = 0.2155$. A section of size $(X, Z) = (48.5, 12.1)$ of the $(L_x, L_z) = (1552, 257.8)$ fracture plane is shown. and $\Delta z = 0.1$. Solution parameters: $\nu = 0.3$, $V = 0.5c_R$, $D = 0.2$, $\psi = 0.5, \Delta z = 0.1$.

Supplementary Video 2 Front dynamics in a checkerboard diamonds toughness pattern. Fronts shown at time intervals $\Delta t = 0.2155$. A section of size $(X, Z) = (42.4, 28.2)$ of the $(L_x, L_z) = (1552, 257.8)$ fracture plane is shown. and $\Delta z = 0.1$. Solution parameters: $\nu = 0.3$, $V = 0.5c_R$, $D = 0.2$, $\psi = 0.5, \Delta z = 0.1$.

Supplementary Video 3 Front dynamics in a checkerboard squares toughness pattern. Fronts shown at time intervals $\Delta t = 0.2155$. A section of size $(X, Z) = (42.4, 28.2)$ of the $(L_x, L_z) = (1552, 257.8)$ fracture plane is shown. and $\Delta z = 0.1$. Solution parameters: $\nu = 0.3$, $V = 0.5c_R$, $D = 0.2$, $\psi = 0.5, \Delta z = 0.1$.

Supplementary Video 4 Front dynamics in a triangular toughness pattern. Fronts shown at time intervals $\Delta t = 0.2155$. A section of size $(X, Z) = (42.4, 28.2)$ of the $(L_x, L_z) = (1552, 257.8)$ fracture plane is shown. and $\Delta z = 0.1$. Solution parameters: $\nu = 0.3$, $V = 0.5c_R$, $D = 0.2$, $\psi = 0.5, \Delta z = 0.1$.

Supplementary Video 5 Front dynamics in a toughness pattern that is the mirror image of Supplementary

Video 4. Fronts shown at time intervals $\Delta t = 0.2155$. A section of size $(X, Z) = (42.4, 28.2)$ of the $(L_x, L_z) = (1552, 257.8)$ fracture plane is shown. and $\Delta z = 0.1$. Solution parameters: $\nu = 0.3$, $V = 0.5c_R$, $D = 0.2$, $\psi = 0.5, \Delta z = 0.1$.

* ikolvin@gatech.edu

- [1] I. Kolvin and M. Adda-Bedia, A comprehensive study of nonlinear perturbations in the dynamics of planar crack fronts (2024), arXiv:2404.18633 [cond-mat, physics:physics].
- [2] L. B. Freund, *Dynamic Fracture Mechanics* (Cambridge University Press, Cambridge; New York, 1990).
- [3] J.-B. Leblond, S. Patinet, J. Frelat, and V. Lazarus, Second-order coplanar perturbation of a semi-infinite crack in an infinite body, *Engineering Fracture Mechanics* **90**, 129 (2012).